Ekman Transport Dominates Local Air–Sea Fluxes in Driving Variability of Subantarctic Mode Water

STEPHEN R. RINTOUL

Antarctic CRC, and CSIRO Division of Oceanography, Hobart, Australia

MATTHEW H. ENGLAND

University of New South Wales, Sydney, New South Wales, Australia

(Manuscript received 5 June 2000, in final form 15 August 2001)

ABSTRACT

Subantarctic Mode Water (SAMW) is formed by deep convection in winter on the equatorward side of the Antarctic Circumpolar Current. Observations south of Australia show that the SAMW temperature (T) and salinity (S) vary significantly from year to year. The magnitude and density-compensating nature of the temperature and salinity changes cannot be explained by variations in air–sea exchange of heat and freshwater in the subantarctic zone where SAMW is formed. Rather, the T and S variability reflects variations in the equatorward Ekman transport of cool, low salinity water across the subantarctic front. Experiments with a coupled climate model suggest that the observations south of Australia are typical of the subantarctic zone. The model changes in SAMW properties are correlated significantly (at 99% level) with changes in wind stress and northward Ekman transport of cool low-salinity water. In contrast, air–sea heat flux anomalies are mostly a response to changes in SST, and anomalies in precipitation minus evaporation in the subantarctic zone are too small to account for the model SAMW salinity variations. Mode waters provide significant reservoirs of heat and freshwater that extend below the depth of the seasonal thermocline and, hence, can persist from year to year. The fact that wind stress variations can drive changes in mode water properties therefore has implications for climate variability.

1. Introduction

Deep convection in winter on the equatorward side of the Antarctic Circumpolar Current (ACC) forms a vertically well-mixed layer known as Subantarctic Mode Water (SAMW). The vigorous winter convection imprints the SAMW with its characteristic properties: a thick layer of uniform density (a pycnostad) and hence low potential vorticity, which is high in oxygen (McCartney 1977). These tracers allow the SAMWs to be tracked from their formation regions in the Southern Ocean to the subtropical gyres, where they renew the waters of the lower thermocline (McCartney 1982). The coldest and freshest varieties of SAMW in the southeast Pacific and southwest Atlantic supply the Antarctic Intermediate Water (AAIW) of those basins (McCartney 1982; Talley 1996). SAMW and AAIW exported from the Southern Ocean form the upper limb of the global overturning circulation (Rintoul 1991; Sloyan and Rintoul 2001b). In addition, SAMW participates in the shallow overturning circulation linking the Pacific and Indian basins, of which the Indonesian Throughflow provides the warm branch and SAMW entering the Pacific south of Australia provides the cool branch (Sloyan and Rintoul 2001a). The formation and export of SAMW also plays an important part in the oceanic uptake and accumulation of gases such as carbon dioxide (CO_2) (Poisson et al. 1993; Metzl et al. 1999; Sabine et al. 1999).

The fact that SAMW ventilates the thermocline of the subtropical gyres and is responsible for uptake and storage of heat, freshwater, and carbon makes variability of SAMW a topic of great interest. Several authors have compared recent and historical hydrographic data and documented changes in the SAMW and AAIW in the interior of the Indian and Pacific Oceans (Bindoff and Church 1992; Johnson and Orsi 1997; Wong et al. 1999; Bindoff and McDougall 2000). These studies suggest that changes in SAMW/AAIW are the result of anomalous air–sea fluxes of heat and freshwater where these layers outcrop; in particular, the widespread cooling and freshening in the SAMW/AAIW density classes is consistent with climate model predictions of warming and/or freshening in the Southern Ocean (Church et al. 1991; Bindoff and McDougall 1994; Banks et al. 2000). However, in the absence of observations in the formation region and a clear physical understanding of the pro-

Corresponding author address: Dr. Stephen R. Rintoul, CSIRO Oceanography, GPO Box 1538, Hobart TAS 7001, Australia.
E-mail: rintoul@drought.ml.csiro.au

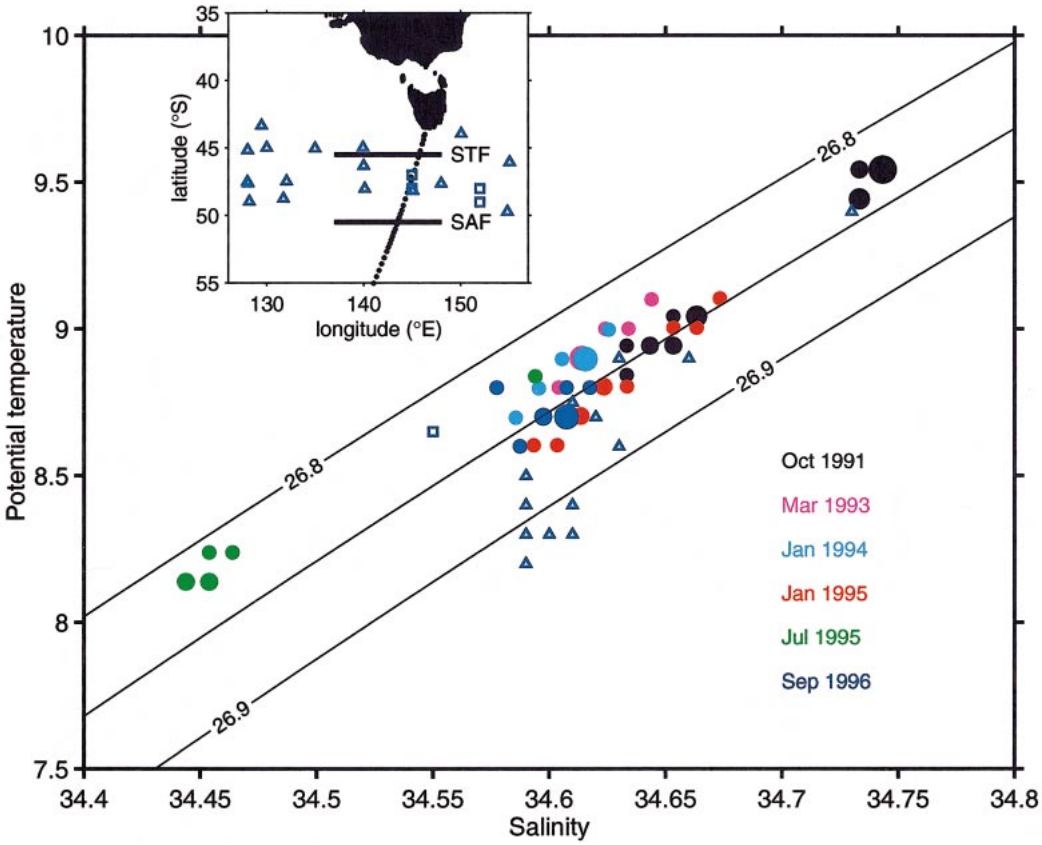

FIG. 1. Variability of SAMW properties south of Australia. The cross-sectional area of water in each 0.1°C by 0.01 psu *T*–*S* class is shown by a filled circle, with the size of the circle proportional to the area. Only the large volume ($>10^7$ m^2) modes are shown. SAMW properties in 1968 (open triangles) and 1978 (open squares) are also shown. Lines are contours of constant potential density. Inset shows the location of the hydrographic section (black dots). SAMW is formed in the SAZ, which is bounded to the north by the STF and to the south by the SAF.

cesses responsible for setting the temperature and salinity of SAMW and AAIW, changes observed away from the formation region can be difficult to interpret.

The traditional view is that the characteristics of SAMW are set by air–sea exchange of heat and freshwater in the subantarctic zone (SAZ). For example, McCartney (1982) attributes the eastward decrease in SAMW temperature and salinity across the Indian and Pacific Oceans to cooling and freshening by air–sea fluxes in the SAZ. England et al. (1993) find that this mechanism operates in a global ocean model, but note that northward Ekman transport also plays a role by carrying cool fresh Antarctic Surface Water into the SAZ where mode water is formed. Here we present observations and model results that show the interannual changes in SAMW temperature and salinity are too large and well-correlated to be the result of anomalous heat and freshwater fluxes in the SAZ. Instead, we demonstrate that changes in ocean transport, in particular cross-frontal Ekman transport driven by variations in wind stress, can explain the observed and modeled SAMW variability.

2. Observations of SAMW variability south of Australia

Six occupations of a repeat hydrographic section between Australia and Antarctica are used to assess the variability of SAMW south of Australia (Fig. 1). The sections were obtained between 1991 and 1996 as part of the World Ocean Circulation Experiment (WOCE, section SR3). The sections cover roughly each season of the year. The water masses and circulation at SR3 are described in Rintoul and Bullister (1999) and transport variability is discussed in Rintoul and Sokolov (2001). Details of the data processing can be found in Rosenberg et al. (1995, 1997).

The variability of SAMW south of Australia is illustrated using an ''area-weighted'' potential temperature–salinity (θ–S) plot (Fig. 1): the cross-sectional area of water within each 0.1°C by 0.01 psu θ–S class is illustrated with a filled circle, whose size is proportional to the area. Only those modes that occupy a significant area ($>10^7$ m^2) of the section are shown. Most of the significant modes lie in a cluster centered on 8.8°C and

34.63 psu, but with a significant range of 0.5°C and 0.1 psu. Two periods have strong modes with properties very different from those of the central cluster. In October 1991, a warm and salty mode (9.5°C, 34.75 psu) was present, as well as a weaker mode with properties similar to the central cluster. In July 1995, an anomalously cold, fresh mode (8.0°C, 34.45 psu) was found, again with a weaker mode near the central cluster. While the range of SAMW properties encountered is large (>1.5°C, 0.3 psu), the temperature and salinity variations tend to be nearly density-compensating.

The properties of SAMW observed on winter cruises in 1968 (Jacobs et al. 1970) and 1978 (Thompson and Edwards 1981) are also included in Fig. 1. The 1978 modes (squares in Fig. 1) observed at 145° and 152°E have the same density as the SR3 modes and are slightly cooler and fresher than the central cluster. The 1968 modes (triangles in Fig. 1) have similar salinities to the central cluster, but their temperatures (and densities) span a wider range than observed in the 1990s. A single station in 1968 has properties close to the warm mode observed in October 1991.

Two examples of the hydrographic structure corresponding to the modes in Fig. 1 are shown in Fig. 2. The thick pycnostad in the upper 600 m is the SAMW. The SAMW is bounded to the north and south by strong meridional gradients of temperature and salinity across the subtropical front (STF) and subantarctic front (SAF), respectively. While the SAMW pool is relatively homogeneous in density (both vertically and horizontally), T and S are less uniform. In both summer (left panels) and winter (right panels), low salinity water spreads equatorward across the SAF in the mixed layer. (The layer of freshwater is thicker in winter because the winter mixed layer depth is deeper.) As a result, the coolest and freshest modes are found in the southern SAZ, and the warmer, more saline modes are found in the northern SAZ.

Local air–sea fluxes of heat and freshwater in the SAZ would be unlikely to combine in such a way as to ensure density-compensating changes in T and S from year to year or within the SAMW pool at a particular time. Moreover, the flux anomalies required to explain the changes in water properties are unrealistically large. Winter mixed layers in this region are approximately 500 m deep [Fig. 2; see also Rintoul and Bullister (1999)]. To cool and freshen a 500-m-thick (by 1 m^2) column by 0.5°C and 0.1 psu (the range of properties observed in the central cluster) requires a heat loss of about 1.0×10^{10} J and a freshwater input of about 1.5 m. If the cooling and freshening were accomplished by flux anomalies maintained for 3 months, the required anomalous rate of heat and freshwater exchange is 130 W m^{-2}, or 5.8 m yr^{-1}. To account for the total range of SAMW T and S observed, anomalous fluxes larger by a factor of 3 would be required. Given that the required anomaly in precipitation minus evaporation ($P - E$) is an order of magnitude larger than the observed winter or annual mean $P - E$, we conclude that the observed variations are unlikely to be solely the result of changes in local air–sea exchange of heat and freshwater.

Advection provides an alternative source of heat and freshwater. In particular, the meridional gradients across the fronts bounding the SAZ are large (Fig. 2), and the strong westerly winds drive a large Ekman flux that is roughly orthogonal to the fronts (Fig. 3). Figure 2 (and in fact each of the WOCE SR3 sections) shows freshwater spreading from south to north across the SAF in the surface mixed layer (Rintoul and Bullister 1999; Rintoul and Trull 2001). Deep winter convection would act to mix the Ekman contribution through the SAMW pool, decreasing the temperature and salinity of the mode water. While the strongest signal of cross-front advection is found near the SAF in the southern SAZ, strong vertical mixing in winter followed by horizontal mixing would act to spread this influence through the SAMW pool.

Before quantifying the role of Ekman advection in the heat balance, we note that, while there are strong gradients in T and S across the SAF in the surface mixed layer, the cross-front density gradient is very weak (Fig. 2). The degree to which the horizontal gradients of T and S are density-compensating is quantified in the upper panels of Fig. 2, by calculating a horizontal density ratio ($R_\rho = \alpha\theta_y/\beta S_y$, where α and β are the expansion coefficients for temperature and salinity, and the temperature and salinity gradients are evaluated between adjacent stations). Values within the SAZ and across the northern part of the SAF are close to $R_\rho = 1$, indicating that the horizontal gradients of T and S make equal and opposite contributions to the horizontal density gradient. Density-compensated fronts have been found in other locations, at a range of space scales (Roden 1977; Rudnick and Ferrari 1999), and the theory of Young (1994) and Ferrari and Young (1997) explains why compensated gradients of temperature and salinity occur in the mixed layer. The important point here is that cross-front advection of cold, fresh water in the mixed layer will change the T and S of SAMW but have relatively little impact on density, consistent with the observed anomalies.

While the focus of this paper is on the temperature and salinity variability of the SAMW, we note in passing that the transport of SAMW south of Australia also varies. Rintoul and Sokolov (2001) find that the transport of SAMW (neutral density 26.9–27.0 kg m^{-3}) across the six SR3 sections ranges from 4 Sv to 16 Sv. (About one-third of this range can be attributed to conversion of some SAMW to lighter density classes by warming in summer.) The temperature and salinity variability described here is largely density-compensating and hence has little impact on the density field and transport.

Following Qiu (2000) and others, we next consider the heat balance in the mixed layer:

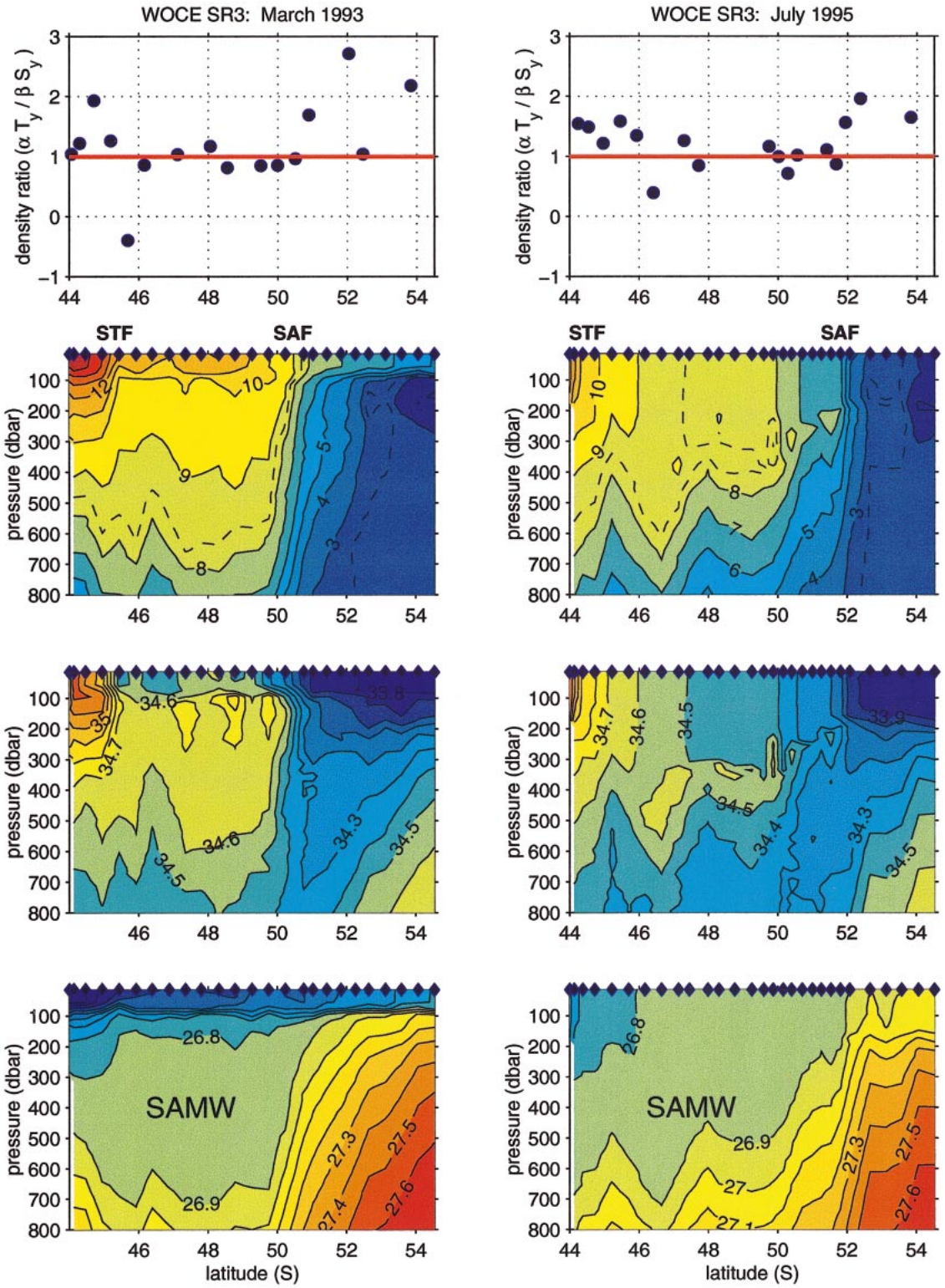

FIG. 2. Property distributions in the SAZ along WOCE section SR3 in Mar 1993 (left panels) and Jul 1995 (right panels). The top row shows the density ratio ($R_\rho = \alpha T_y/\beta S_y$), evaluated by taking differences in mixed layer temperature and salinity between adjacent stations; points are plotted when the horizontal salinity gradient (S_y) is greater than 0.02 psu. The second row is potential temperature (contour interval 1°C; the 8.5° and 2.5°C contours are dashed); third row is salinity (contour interval 0.1 psu); fourth row is potential density (contour interval 0.1 kg m^{-3}). Station positions are indicated by diamonds at the top of each plot.

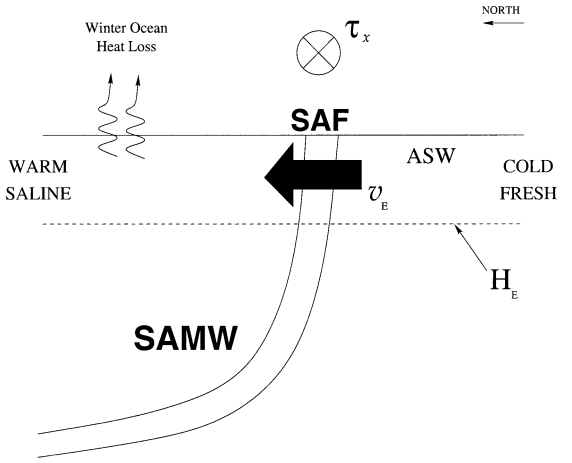

FIG. 3. Schematic diagram showing cross-front Ekman transport driven by westerly winds over the Southern Ocean. Cold fresh ASW is advected in the surface Ekman layer H_E at a rate υ_E across the SAF. Ocean–atmosphere heat loss during winter can also act to cool SAMW. Lines represent isotherms outcropping at the SAF.

$$\frac{\partial T_m}{\partial t} = \frac{Q_{\text{net}}}{\rho_o c_p h_m} - \mathbf{u}_e \cdot \nabla T_m - \frac{w_e(T_m - T_d)}{h_m} - \mathbf{u}_g \cdot \nabla T_m, \quad (1)$$

where T_m is the mixed layer temperature, Q_{net} is the net air–sea heat exchange, ρ_o is density, c_p is the specific heat, h_m is the mixed layer depth, $\mathbf{u}_e$ is the Ekman velocity, w_e is the entrainment velocity, T_d is the temperature below the mixed layer, and $\mathbf{u}_g$ is the geostrophic velocity.

We do not have sufficient information to evaluate each of the terms in the temperature tendency equation from the observations (e.g., T_m, h_m, and w_e are not known as a function of time). However, we can roughly estimate each of the terms and get a feeling for the likely lowest-order balance in the SAZ.

Surface heat flux: The mean winter (June, July, August average) ocean heat loss over the SAZ south of Tasmania is about 75 W m^{-2} (Josey et al. 1998). Most of this heat loss goes to remove the warm seasonal thermocline produced during the preceding summer (the annual mean exchange is a heat gain of +15 W m^{-2}) and interannual anomalies in winter cooling, though poorly known, are likely smaller than the mean heat loss. However, for the sake of estimating terms, if we apply the full mean winter heat loss to changing the temperature of the 500-m-thick winter mixed layer, we obtain a temperature tendency of -4×10^{-8}°C s^{-1} (using $\rho_o = 1027$ kg m^{-3} and $c_p = 3986$ J kg^{-1} K^{-1}).

Ekman advection: Interannual anomalies of monthly mean zonal wind stress near 50°S, 140°E are about 0.1 N m^{-2} (Kalnay et al. 1996). A zonal wind stress anomaly of 0.1 N m^{-2} at this latitude results in a northward Ekman velocity anomaly of about 0.01 m s^{-1} (assuming an Ekman layer thickness of 100 m). A typical meridional temperature gradient across the SAF is 3°C/100 km. Ekman advection therefore results in a temperature tendency of about -3×10^{-7}°C s^{-1}.

Vertical entrainment: Vertical entrainment is unlikely to contribute much to the temperature tendency. In order to entrain cooler water from beneath the base of the winter mixed layer, the density of the entire vertical column of SAMW must be increased. To change the density of the thick SAMW pycnostad requires a large buoyancy loss, which we have shown does not occur in this region.

Geostrophic advection: We assume the meridional geostrophic velocity is weak because the changes in density along the SAF are small. Based on the SR3 sections, maximum anomalies of zonal geostrophic surface current in the SAZ are about 0.1 m s^{-1} (relative to the bottom). To estimate the zonal gradient of T_m, we note that the SAMW on the WOCE I9 section at 115°E has a mean temperature of about 9.5°C, giving a zonal temperature gradient of 0.7°C/2100 km. The zonal advection contribution to the temperature tendency is therefore about 3×10^{-8}°C s^{-1}.

The Ekman heat advection is roughly an order of magnitude larger than the other terms in the heat balance, suggesting that the lowest-order balance is between the temperature tendency and Ekman advection.

Alternatively we can consider a simple heat and salt budget for the southern SAZ to evaluate how much cool fresh Antarctic Surface Water (ASW) from south of the SAF must be added to account for the observed anomalies. Conservation of heat and salt requires $V_oT_o + V_eT_e = V_fT_f$ and $V_oS_o + V_eS_e = V_fS_f$, where (V_o, S_o, T_o), (V_f, S_f, T_f), and (V_e, S_e, T_e) are the initial, final, and Ekman values of volume, salinity, and temperature. Solving for V_e, we find that an addition of ASW equal to 9% of the initial mode water volume is sufficient to cool the mode water pool by 0.5°C (assuming T_o = 9.0°C, T_f = 8.5°C, and T_e = 3.0°C). Similarly, a 0.1-psu freshening requires a volume of ASW equal to 14% of the original volume (S_o = 34.6 psu, S_f = 34.5 psu, S_e = 33.8 psu). A wind stress anomaly to 0.1 N m^{-2} maintained over three months would drive enough ASW across the front to dilute the SAMW in the southern SAZ by about 11% (using the fact that the cool, fresh modes found in the southern SAZ are typically about 300 m thick and 200 km wide; Fig. 2).

Other changes in ocean transport may contribute to the observed SAMW variability. Rings and filaments pinched off from the fronts bounding the SAZ may also play a role; for example, the three isolated salinity maxima near 150 dbar seen in the March 1993 section (Fig. 2) are the result of intrusions of subtropical water entering the SAZ from the north. Similarly, repeat XBT sections through this region often cross cold-core rings that have pinched off the SAF and entered the SAZ (Rintoul et al. 1997). The rings extend from the surface to the seafloor and represent a large freshwater anomaly in the SAZ. Note, however, that the water from south of the SAF that forms the core of these rings is denser

than the water in the SAZ itself, so the pinched off rings would change the density as well as the *T* and *S* of the SAMW. The fact that the density of the SAMW does not change much with time suggests that ring-shedding events are not frequent enough to play a major role in the heat and salt balance.

The observations discussed above show that the temperature and salinity of SAMW south of Tasmania changes significantly from year to year and that these changes are nearly density-compensating. Simple budget calculations suggest that variations in Ekman transport across the SAF are the most likely explanation for the observed variability. However, the lack of repeat sections at other longitudes prevents us from determining whether the measurements south of Australia are representative of the circumpolar SAZ region. To address this question, and to further test the hypothesis that Ekman transport influences SAMW properties, we next consider SAMW variability in a coupled climate model.

3. SAMW variability in a coupled climate model

Typical variability in SAMW properties in the coupled climate model of Manabe and Stouffer (1996) is shown in Fig. 4, which shows a multicentury time series of *T–S* in the winter mixed layer at 48°S near the SR3 line. The model consists of coupled atmosphere–ocean–ice–land surface components and includes a seasonal cycle in solar insolation [see Manabe and Stouffer (1996) for a detailed description of the model]. The ocean component of the model has 12 vertical levels and approximately 4° horizontal resolution. While the model is of very coarse resolution, it has the advantage that it can be run in coupled mode for long periods (in this case 1000 yr) to assess the ''natural variability'' of the modeled ocean–atmosphere system. Manabe and Stouffer (1996) have demonstrated that the model captures observed scales of interannual variability rather well, though with reduced ENSO amplitude. Of relevance here is the model's representation of the Southern Ocean. The ACC in the model appears as a single band of enhanced meridional SST gradient, rather than as a number of distinct fronts as observed. North of the ACC, deep mixed layers are formed, the model analog of SAMW (Fig. 5). Mesoscale eddies cannot be resolved by the coarse model; instead, isopycnal mixing and a background horizontal diffusion are used to parameterize the effect of subgrid-scale motions.

The *T–S* plot included in Fig. 4 shows late winter SAMW properties at four locations: (i) near the SR3 line (48°S, 145°E), (ii) in the southeast Indian Ocean (52°S, 103°E), and (iii), (iv) in the southeast Pacific Ocean (56°S, 133°W and 100°W). A *T–S* point is drawn when the winter mixed layer is deeper than 300 m. The temperature range in mode waters at SR3 is about 2°C, a little higher than that observed. This is to be expected, as the 1000-yr model run covers a much longer time period than the six years of observations. The model salinity range at SR3 is 0.3 psu, which is about what was observed during the 1990s repeat sections. The model root-mean-square (rms) variability in SAMW properties at this location is 0.45°C and 0.07 psu. Variability in *T–S* at the other longitudes shown is a little weaker. Nevertheless, at each location variations in *T* and *S* tend to be nearly density-compensating. The time series of SAMW *T* and *S* at the model grid point near SR3 (Figs. 4a,b) shows that the anomalies occur at a range of timescales, from interannual to centennial.

In the model, open ocean convection and mode water formation is generally more widespread than in observations (see, e.g., England 1995). This in part explains why a variety of mode water at 103°E is a little cooler and fresher than the mode water at the SR3 line, in spite of being west (or ''upstream'') of the southwest Pacific transect. One grid point to the north of the 52°S, 103°E location, shown in Fig. 4c, mode waters are generally warmer and more saline than at the SR3 line. The overall trend of eastward cooling and freshening of SAMW is reproduced by the model, but at most longitudes there is a relatively large *T–S* range in the convected mixed layer.

Further analyses of upper-ocean water mass variability in the climate model suggest that *T–S* anomalies are generally density compensating over much of the midlatitude Southern Ocean. Figure 6 shows the local correlation between late winter sea surface temperature and salinity over the Southern Hemisphere for 1000 years of model data. The late winter period is chosen because that is when SAMW properties are exposed at the sea surface. Winter SST and SSS are highly positively correlated over an extensive region, with warm temperature anomalies at 40°–60°S accompanied by higher salinity, and cool anomalies coinciding with low salinity. This pattern excludes the possibility that latent (evaporative) heat loss controls SST variability, as then SST and SSS would be negatively correlated (as occurs in the Tropics, where such fluxes play a greater role in altering surface *T–S* properties).

It remains to be seen what processes control the variability of mode water properties in the model and whether these vary with geographic location. The positive *T–S* correlations seen in Fig. 6 could be a result of ocean advection (meridional or zonal) or could result from variations in incoming solar radiation being tied to anomalous rainfall patterns (via storm cloud cover effects). Both mechanisms would give rise to *T* and *S* anomalies occurring in phase, and in the same sense (see also Fig. 3).

We now investigate the role of surface heat flux anomalies in determining SAMW temperature change in the model. The traditional view is that the temperature of SAMW is set by wintertime ocean heat loss in the SAZ. Figure 7 shows the correlation between the integrated winter (June, July, August) ocean–atmosphere heat loss and the late-winter (September) SST. If variability in

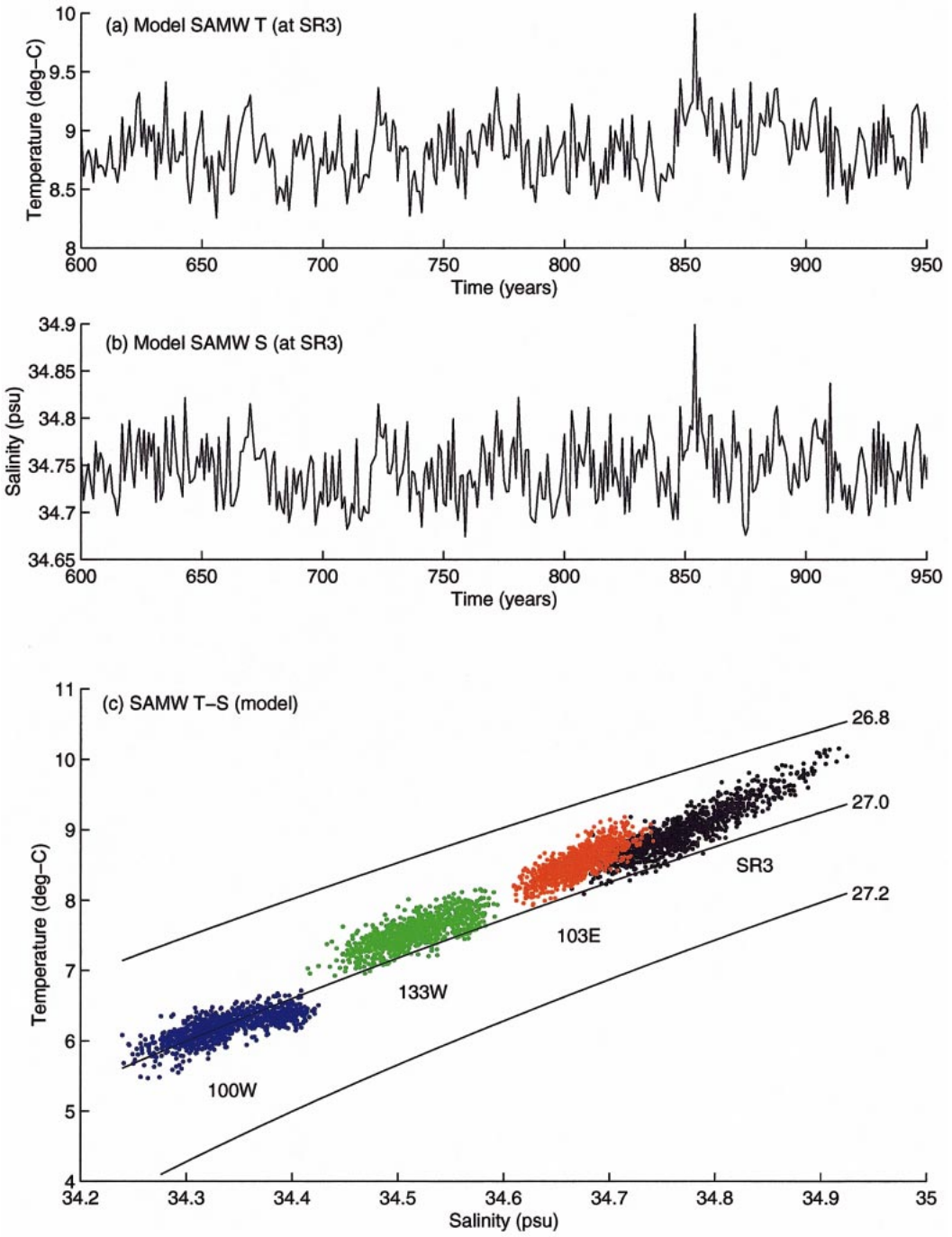

FIG. 4. (a), (b) Time series of $T - S$ in a deep mixed layer near 48°S, 145°E for a 350-yr period, from a 1000-yr run of a coupled climate model. (c) *T–S* scatterplot in the late-winter mixed layer at four locations: 145°E (near the SR3 line), 103°E, 133°W, and 100°W.

air–sea heat fluxes is controlling changes in SAMW temperature, we would expect to see low temperatures follow higher-than-average ocean heat loss during the preceeding winter (i.e., negative correlations). However, this is not the case: SAMW temperatures tend to correlate *positively* with ocean heat loss (i.e., colder SAMW occurs after a winter of lower-than-average ocean heat loss). While this might at first appear to be contradictory, it should be noted that the dominant timescale of SST variability in the region is interannual. Thus, anomalous SST patterns persist for seasons to years, being damped slowly by local air–sea heat fluxes. This ex-

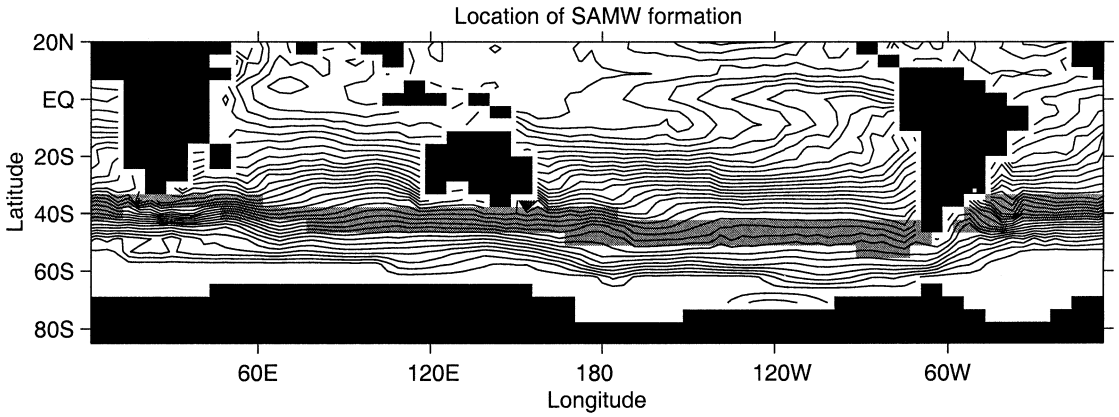

FIG. 5. Location of SAMW formation in the coupled climate model. A grid box is selected wherever there is regular formation of thick winter mixed layers (to depths of 250–500 m) on the northern flank of the ACC. Overlaid are contours of mean Sep SST averaged over 100 years of simulation time (with contour interval 1°C).

plains why the net winter ocean heat loss and late-winter SST are for the most part positively correlated: cool (warm) winter SST anomalies result in low (high) heat loss from the ocean. As such, SST anomalies are seen to drive surface heat flux variations in the model, not the other way around.

We next turn our attention to the role of wind-driven Ekman transport variability in driving SAMW temperature anomalies. Figure 8 shows the correlation between annual mean SST and annual mean northward Ekman velocity v_e. Annual mean values were chosen in this analysis because, as above, the dominant model timescale of variability is interannual. The Ekman velocity is calculated as $v_e = \tau_x/(\rho_o f h_m)$ with h_m taken to be the depth of the surface layer in the model (50.9 m). The latitude at which v_e is examined is offset by approximately 2° to the south of the SST grid point (due to the model grid system). Year-to-year changes in the wind-driven Ekman velocity v_e (positive northward) are highly negatively correlated with changes in SST. When the wind increases, northward Ekman velocities increase, carrying more cool low-salinity Antarctic surface waters across the SAF. As a result, anomalies in wind stress and meridional Ekman flow correlate negatively with SST and SSS. The model subgrid-scale diffusion also contributes by mixing water across the front. During times of weaker westerlies, SAMW comprises less Antarctic Surface Water, and instead includes more water

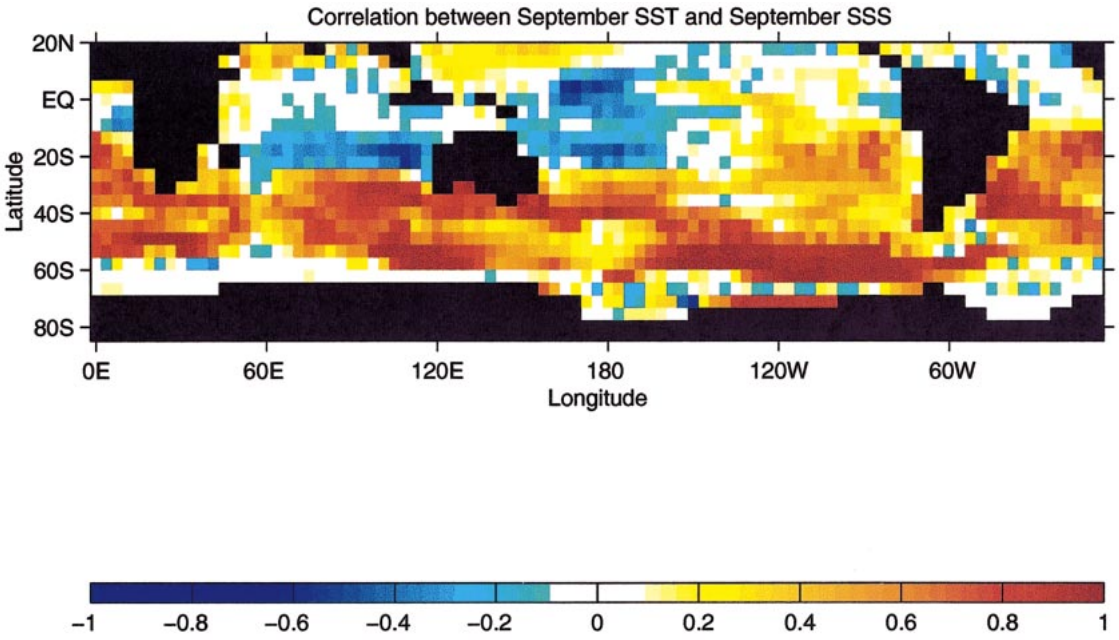

FIG. 6. Correlation between Sep SST and Sep SSS over the Southern Hemisphere for 1000 years of model data. Model grid regions are only shaded where the correlation is statistically significant (at 99% level).

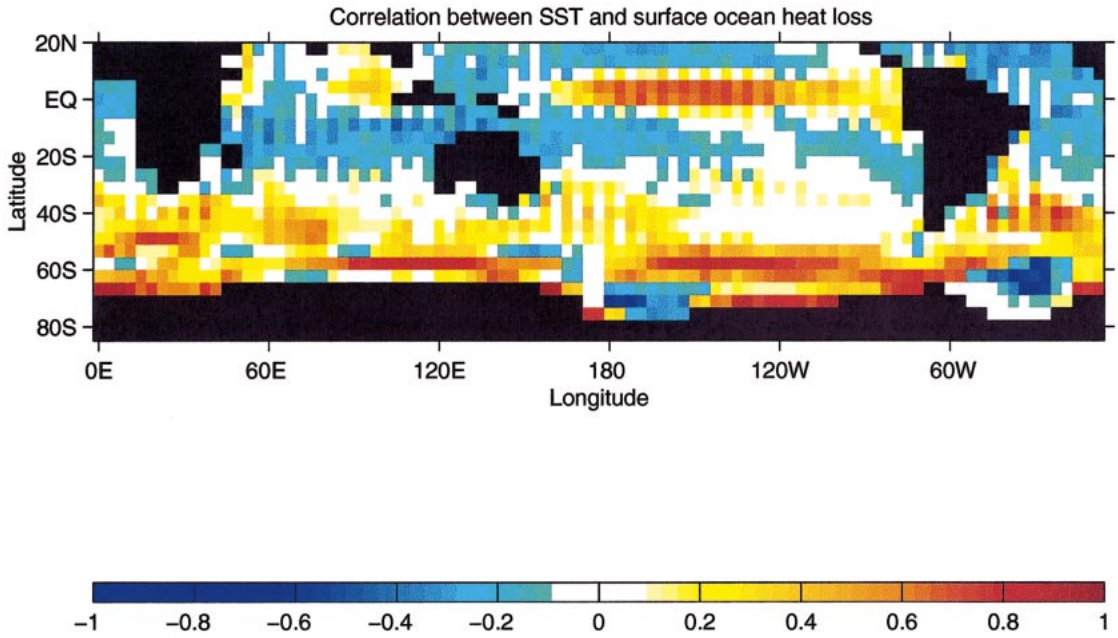

FIG. 7. Correlation between integrated winter (Jun–Jul–Aug) ocean–atmosphere heat loss and late-winter (Sep) SST for 1000 years of model data. Model grid regions are only shaded where the correlation is statistically significant (at 99% level).

of subtropical origin (with higher *T–S*). Variability in the amount of warm, saline water carried poleward in the western boundary currents thus can also affect SAMW *T–S*. Because the property changes are largely density-compensating (Fig. 4c), the model shows only weak variations in SAMW mixed layer depths.

In addition to these meridional advection effects, upper-ocean *T–S* anomalies in the model are advected eastward by the ACC. Anomalous westerlies drive variations in northward Ekman transport and SAZ *T–S* in one region; the anomalous SAMW then gets transported eastward by the background flow field. While air–sea

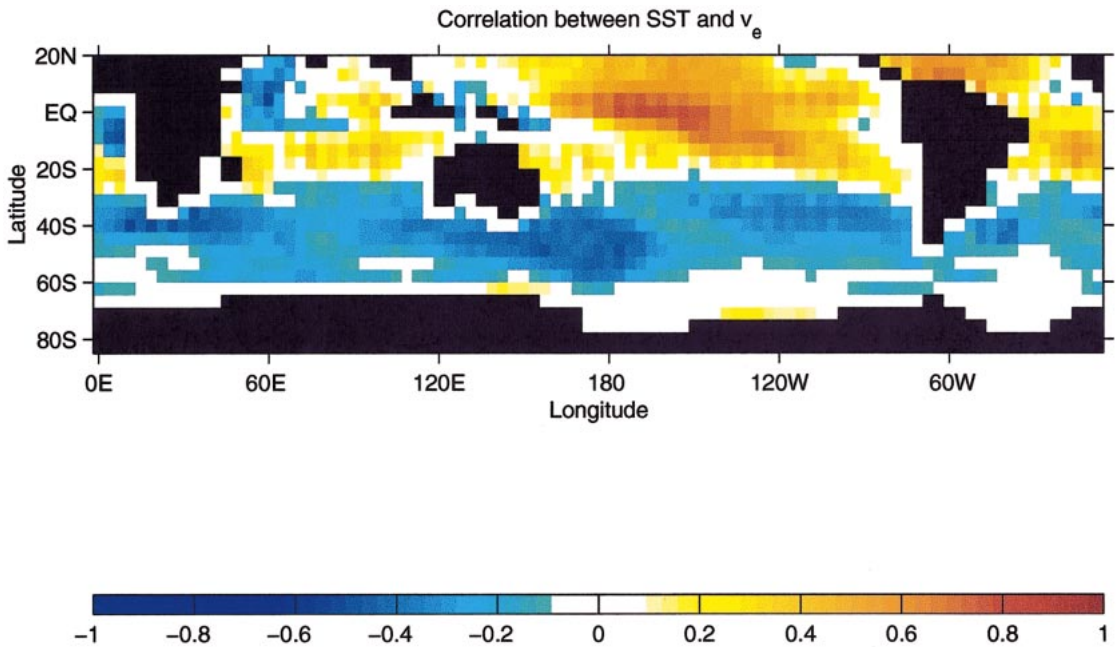

FIG. 8. Correlation between annual mean SST and north–south surface Ekman velocity v_e. Model grid regions are only shaded where the correlation is statistically significant (at 99% level).

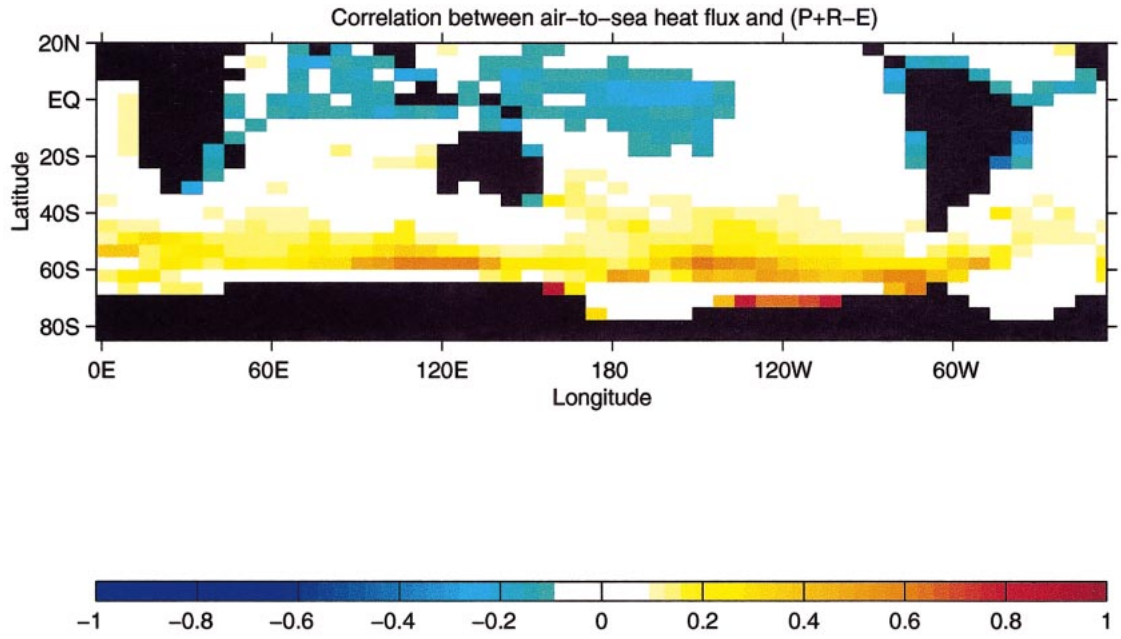

FIG. 9. Correlation between net air-to-sea heat flux anomalies and precipitation plus runoff minus evaporation ($P + R - E$). Model grid regions are only shaded where the correlation is statistically significant (at 99% level).

heat exchange will act to damp out this signal, variability can be detected downstream from the original wind stress anomaly region (over the order of thousands of kilometers, figure not shown). The correlation analysis shown in Fig. 8 does not include this process as it only *locally* correlates SST variations with north–south Ekman velocity.

Figure 8 suggests that northward Ekman transport variability might drive density-compensating anomalies in SAMW *T–S.* It is possible that air–sea heat and freshwater flux variations *south* of the SAF might also act in such a way to alter *T* and *S* in phase, with the resulting anomalies advected northward by the mean Ekman flow across the SAF. For example, rainfall and cloud cover variability could alter *T–S* in phase. To examine this possibility, we calculate the local correlation between net air-to-sea heat flux anomalies and precipitation plus runoff minus evaporation ($P + R - E$; Fig. 9). Negative correlations occur where increased ocean heat loss is in phase with high rainfall (e.g., due to storms), whereas positive correlations indicate that increased ocean heat loss occurs in phase with high evaporation (i.e., due to latent heat fluxes). Nowhere in the Southern Ocean do anomalies in net surface heat fluxes combine with $P - E$ fluxes to generate ''in-phase'' *T–S* variability. In fact, the dominant coherent pattern of variability is that due to evaporative fluxes, which tend to change *T–S* in a non-density-conserving fashion. Variability in sea ice formation (not included in Fig. 9) would also likely act to create non-density-conserving *T–S* anomalies (i.e., warming and ice melt produce warm, fresh anomalies; freezing creates cold, salty anomalies). Thus, air–sea and ocean–ice fluxes cannot account for the density-compensating nature of SAMW anomalies in the model.

The above analyses of correlation statistics show (i) that variations in meridional Ekman transport are in phase with anomalies in SST, (ii) that winter ocean heat loss tends to vary in response to interannual surface *T* anomalies, and (iii) that air–sea flux variations south of the SAF cannot account for the density-conserving nature of *T–S* anomalies in the model. It remains to be seen whether the magnitude of variability of northward Ekman advection is sufficient to account for changes in heat content in SAMW. Table 1 shows the standard deviation and correlation coefficients of heat budget terms for Subantarctic Mode Waters averaged between 120° and 160°E. The statistics are calculated from 100 years of the climate model run. Correlation coefficients are calculated versus the *T* tendency term $\partial T_m/\partial t$. From the standard deviations it is clear that the variability in meridional Ekman advection is large enough to account for SAMW heat content variability in the model. In contrast, the zonal advection, vertical mixing, and zonal diffusion play a much lesser role in generating *T* variability. Furthermore, only the meridional advection and meridional diffusion terms are correlated significantly with the heat storage rate. The other terms are either too small in magnitude or not significantly in phase with $\partial T_m/\partial t$.

Table 1 suggests that anomalies in north–south Ekman transport largely drive anomalies in *T.* Zonal advection can also contribute by carrying anomalous heat content eastward, though variability in this term is a factor of 4 smaller than variability in the meridional advection

TABLE 1. Standard deviation and correlation coefficients of temperature budget terms for SAMW averaged between 120° and 160°E. The standard deviations are calculated from 100 years of the model run. Correlation coefficients are calculated vs the T tendency term $\partial T_m//\partial t$. Statistics are computed from the time series of regionally averaged interannual tracer tendency terms. Other subregions of the circumpolar ocean exhibit similar patterns, with variability in meridional advection greater than zonal advection and subduction. Significant variability in meridional mixing is due to Ekman-driven fluctuations in surface T yielding different cross-front diffusion rates. Correlation coefficients above 0.26 are significant at the 99% confidence level (shown boldface).

Budget term	Standard deviation ($\times 10^{-8}$°C s^{-1})	Correlation with $\partial T_m/\partial t$
$\partial T_m/\partial t$	2.28	1.00
Net surface heat flux	1.68	0.13
Zonal advection, $u\partial T/\partial x$	0.84	0.22
Meridional advection, $v\partial T/\partial y$	3.61	**0.36**
Meridional Ekman advection[a]	3.45	**0.39**
Vertical advection, $w\partial T/\partial z$	1.79	−0.03
Zonal diffusion[b]	0.31	0.11
Meridional diffusion[b]	2.26	**0.37**
Vertical mixing[c]	0.64	0.03

[a] The meridional Ekman advection is calculated using a north–south Ekman velocity $v_E = -\tau_x/\rho hf$, where τ_x is zonal wind stress, ρ is density, h is the upper-layer thickness, and f is the Coriolis parameter.

[b] Zonal and meridional diffusion terms include the Geophysical Fluid Dynamics Laboratory (GFDL) model isopycnal and background horizontal mixing components. It may be noted that in the north–south sense, this term is dominated by the background horizontal mixing component.

[c] The vertical mixing is the sum of convective overturn effects, isopycnal stirring, and explicit vertical diffusion.

TABLE 2. As in Table 1 but for the salinity budget terms. Correlation coefficients are calculated vs the S_m tendency term $\partial S_m/\partial t$. Correlation coefficients above 0.26 are significant at the 99% confidence level (shown boldface).

Budget term	Standard deviation ($\times 10^{-9}$ psu s^{-1})	Correlation with $\partial S_m/\partial t$
$\partial S_m/\partial t$	1.87	1.00
Net surface freshwater flux	1.42	**−0.29**
Zonal advection, $u\partial S/\partial x$	1.04	0.20
Meridional advection, $v\partial S/\partial y$	2.57	**0.41**
Meridional Ekman advection	2.40	**0.48**
Vertical advection, $w\partial S/\partial z$	1.65	−0.11
Zonal diffusion	0.21	0.14
Meridional diffusion	1.05	**0.45**
Vertical mixing	0.58	−0.04

term. The meridional diffusion scales as $\partial^2 T/\partial y^2$ in the model and, as such, can be interpreted as a term that damps out localized heat content anomalies. The meridional diffusion rates vary in phase with $v_e\partial T_m/\partial y$ and $\partial T_m/\partial t$, as the mixing rate is directly related to the north–south T structure that is in part set by local Ekman transport rates. In other words, the budget terms are not independent (e.g., changes in Ekman transport yield changes in $\partial T_m/\partial y$ and thus changes in meridional diffusion).

Other subregions of the circumpolar ocean exhibit similar patterns: variability in meridional (largely Ekman) advection is greater than variability in zonal or vertical advection and, importantly, is in phase with SAMW T variability. The significant variability in meridional mixing is due to Ekman-driven fluctuations in surface T yielding different cross-front diffusion rates. Variability in surface heat fluxes is about 75% of the magnitude of heat content variability in SAMW; only it is the SST changes that drive the heat flux variability, not the other way around (see also Fig. 7).

A similar set of correlation and standard deviation analyses for upper-ocean salinity is included in Table 2. The calculations show that the variability in model salinity is also controlled by Ekman-driven advection, though notably the surface freshwater ($P - E$) flux does account for some variability as well. This is to be expected as, unlike heat, there is negligible feedback between surface salinity anomalies and air–sea fluxes. Thus, freshwater flux–driven S anomalies can persist in the ocean for longer periods of time. It may be noted, however, that the magnitude of variability in ($P - E$) is about half that of the Ekman advection term, and variations are not as highly correlated with $\partial S_m/\partial t$. In summary, variability in SAMW S is controlled by (i) changes in the strength of the northward Ekman transport, (ii) changes in S due to net evaporation/precipitation either side of the SAF (those to the south are advected into the SAMW formation region by Ekman flow), and (iii) eastward advection of upper-ocean S anomalies [whether originally a result of (i) or (ii)]. Meridional diffusion is the main process responsible for local damping of the SAMW salinity anomalies.

4. Summary and discussion

Observations and results of a coupled model show that the temperature and salinity of SAMW vary significantly from year to year. The changes are nearly density-compensating so that the depth of winter mixing and SAMW density do not change much with time. The magnitude of the temperature and salinity changes is too large to be explained by anomalies in local air–sea exchange of heat and freshwater. This result might have been anticipated from Warren (1972), who showed that the temperature and salinity of mode waters were likely to be insensitive to meteorological fluctuations due to their great thickness and because much of the cooling season is spent removing the seasonal thermocline. Rather, anomalous advection of temperature and salinity in the Ekman layer in response to changes in zonal wind stress appears to cause the observed and modeled SAMW anomalies. Other terms in the heat and freshwater budgets (e.g., air–sea fluxes, zonal advection, cross-front mixing) also contribute but play a lesser role.

While the focus of this paper is on the variability of SAMW, the mean SAMW properties at any longitude also likely reflect the input of cold, fresh water provided

by the mean Ekman transport. In particular, the gradual cooling and freshening of SAMW across the Indian and Pacific Oceans can be explained at least in part by Ekman advection across the SAF, rather than solely by air–sea fluxes in the SAZ as suggested by McCartney (1982). Recently, Ribbe (1999) analyzed a series of idealized ocean model experiments with differing subantarctic wind stress fields to show how changes in northward Ekman transport can affect SAMW *T*–*S* properties. The ''overrunning'' of the SAF by cool, fresh waters from the south, which we have interpreted as the signature of cross-front Ekman transport, is a common feature in Southern Ocean sections; similar features are observed in sections across the subarctic front in the North Pacific (e.g., Roden 1977), suggesting that cross-front Ekman advection may also be important there. Diagnostic calculations, which account for water mass transformation driven by air–sea buoyancy fluxes, also show that water crossing the SAF from the south contributes to the formation of SAMW (Speer et al. 2000; Sloyan and Rintoul 2001a).

Temperature and salinity anomalies in other regions where strong winds blow parallel to oceanic fronts (e.g., the North Pacific and North Atlantic) may also be driven by wind stress anomalies via the Ekman mechanism. For example, Yasuda and Hanawa (1997) conclude that Ekman advection makes a significant contribution to decadal variations in mode water temperatures in the North Pacific. The North Pacific and North Atlantic regions of the coupled model do in fact exhibit variability in SST and SSS, which is significantly correlated with wind stress variations (not shown). Using a coupled model of comparable resolution, Watterson (2000) also found that vacillations in southern midlatitude zonal winds drove SST anomalies via anomalous Ekman advection.

Several recent explanations of decadal variability in midlatitudes rely on the memory provided by ocean temperature anomalies that extend beneath the summer mixed layer (e.g., Latif and Barnett 1994; Sutton and Allen 1997). Anomalous Ekman heat advection may play a more significant role than previously appreciated in producing and maintaining the SST anomalies that participate in the feedback system responsible for such instabilities. In his classic paper on air–sea interaction in the North Atlantic, Bjerknes (1964) found a strong correlation between SST anomalies in the North Atlantic and the strength of the westerlies. He attributed the cooling during periods of strong westerly winds to enhanced latent heat loss. The fact that the largest SST anomalies are found along the strong SST gradient associated with the North Atlantic Current (e.g., near 50°N, 35°W) is, however, also consistent with anomalous Ekman advection. Bjerknes (1964, p. 62), in fact, noted such a possibility when discussing changes in SST near the Gulf Stream between the 1920s and 1930s, but in general he believed the effect of winds on latent heat exchange to be the dominant mechanism. Indeed, one might expect the Ekman mechanism to make a relatively smaller contribution in the Northern Hemisphere, due to the difference in continental geometry in the two hemispheres: the northern basins experience outbreaks of cold, dry continental air in winter, which drive large air–sea fluxes; the more maritime southern basins experience weaker air–sea fluxes. The strong poleward flow of warm water in the Gulf Stream and Kuroshio means that geostrophic heat advection is also likely to be a more significant term in the heat budget in the North Atlantic and North Pacific (e.g., Qiu 2000) than in the Southern Ocean.

One example of a coupled phenomenon that may involve anomalous Ekman advection is the Antarctic Circumpolar Wave (ACW). The ACW is a zonal wavenumber 2 pattern of anomalies in sea surface temperature, sea surface height, sea level pressure, and sea ice extent that circles Antarctica in about 8–10 years (White and Peterson 1996; Jacobs and Mitchell 1996). A number of simple analytical coupled models have recently been proposed to explain the physical mechanism behind the ACW. In many of these models, meridional advection of the mean sea surface temperature gradient plays a role in the dynamics (White et al. 1998; Talley 1999; Baines and Cai 2000). Only the White et al. (1998) study explicitly considers Ekman advection, and none of the existing models accounts for the large SST gradients associated with the jets of the ACC. Our results suggest that meridional Ekman advection acting on the sharp SST gradients at the ACC fronts is likely to be an effective means of driving changes in SST and heat content, and therefore likely to make an important contribution to the ACW. A realistic representation of Southern Ocean fronts may be necessary to capture the essence of the physical mechanism behind the ACW.

The dominance of Ekman transport over air–sea flux anomalies in driving SAMW variability has implications for the interpretation of differences between repeated hydrographic sections. Comparisons of hydrographic sections taken decades apart tend to show cooling and freshening on isopycnals over large parts of the southern Indian and South Pacific Oceans (Bindoff and Church 1992; Johnson and Orsi 1997; Wong et al. 1999; Bindoff and McDougall 2000). The cooling and freshening signal is largest in the SAMW. Following the arguments of Church et al. (1991), such changes have been interpreted as the signature of warming and/or freshening in the SAMW formation region. However, as demonstrated here and in Warren (1972), local air–sea flux anomalies are unlikely to drive significant changes in the *T* and *S* of the thick SAMW layer. Transport of cool, fresh water across the SAF provides an alternative, and likely more potent, means of changing the *T* and *S* on isopycnals.

The Ekman mechanism would operate in a similar manner in a climate change scenario. Long-term changes in the strength, location or orientation of the wind stress relative to the SAF could drive basin-scale changes in the *T* and *S* of mode waters. (Such changes in the

wind would of course have a number of other potential consequences, including changes in the rate of Ekman divergence and convergence and, hence, subduction and the transport of the ACC, but the focus here is on water mass variability.) This suggests that the pattern of large-scale cooling and freshening observed in the studies referred to above might be explained by a decadal-scale increase in the westerly winds over the Southern Ocean.

However, there are some difficulties with this interpretation. Observations are scarce over the Southern Ocean, so it is difficult to say whether the wind stress has changed significantly in recent decades. The 1963–83 wind stress anomaly (relative to the 1900–83 annual mean) is generally weak between 40° and 46°S (Reason 2000), but the maps do not extend south of 46°S due to data limitations. Perhaps more importantly, observations within the SAMW formation region south of Australia do not show evidence of significant changes on decadal timescales: the SAMW formed in 1968 and 1978 falls close to the central cluster of observations observed in the 1990s (Fig. 1). It is also not clear how the significant interannual variability found in our observations and model could get averaged out, so only the signal of the trend remains in the ocean interior. On the other hand, the consistent pattern observed in several basins (e.g., Wong et al. 1999) and simulated in climate models (e.g., Banks et al. 2000) is difficult to dismiss as aliased higher frequency variability. More high quality repeat sections are required to determine the patterns, timescale, and likely causes of changes in the ocean interior. Our results suggest that measurements of change in the ocean interior will remain difficult to interpret in the absence of observations in the water mass formation regions.

Mode waters such as SAMW play a number of key roles in the climate system. SAMW and AAIW ventilate the waters of the lower thermocline of the Southern Hemisphere gyres and in this way influence the capacity of the gyres to store heat, carbon, and freshwater (Gordon 1991). The deep winter mixed layers persist from one winter to the next beneath the shallow summer pycnocline and so provide a memory that extends beyond seasonal timescales. The persistent and volumetrically significant reservoirs of heat and freshwater provided by mode waters may play a part in mechanisms of interannual and decadal variability. For these reasons, knowledge of how and why the properties of SAMW vary with time is required to understand climate variability. Our results suggest that ocean transport, in particular Ekman transport across oceanic fronts, plays the dominant role in driving variability of SAMW.

Acknowledgments. Ron Stouffer kindly provided data from the GFDL climate model control simulations. Helpful comments on an earlier draft were provided by John Church, Nathan Bindoff, Trevor McDougall, Stuart Godfrey, Chris Reason, and two anonymous reviewers. Mark Rosenberg calibrated and processed the CTD data. Model graphics were prepared by Elena Goloubeva. This work is supported in part by Environment Australia through the National Greenhouse Research Program and in part by the Australian Research Council.

REFERENCES

Baines, P. G., and W. Cai, 2000: Analysis of an interactive instability mechanism for the Antarctic Circumpolar Wave. *J. Climate,* **13,** 1831–1844.

Banks, H. T., R. A. Wood, J. M. Gregory, T. C. Johns, and G. S. Jones, 2000: Are observed decadal changes in intermediate water masses a signature of anthropogenic climate change? *Geophys. Res. Lett.,* **27,** 2961–2964.

Bindoff, N. L., and J. A. Church, 1992: Warming of the water column in the southwest Pacific Ocean. *Nature,* **357,** 59–62.

——, and T. J. McDougall, 1994: Diagnosing climate change and ocean ventilation using hydrographic data. *J. Phys. Oceanogr.,* **24,** 1137–1152.

——, and ——, 2000: Decadal changes along an Indian Ocean section at 32°S and their interpretation. *J. Phys. Oceanogr.,* **30,** 1207–1222.

Bjerknes, J., 1964: Atlantic air–sea interaction. *Advances in Geophysics,* Vol. 10, Academic Press, 1–82.

Church, J., J. Godfrey, D. Jackett, and T. McDougall, 1991: A model of sea level rise caused by ocean thermal expansion. *J. Climate,* **4,** 438–456.

England, M. H., 1995: Using chlorofluorocarbons to assess ocean climate models. *Geophys. Res. Lett.,* **22,** 3051–3054.

——, J. Godfrey, A. Hirst, and M. Tomczak, 1993: The mechanism for Antarctic Intermediate Water renewal in a World Ocean model. *J. Phys. Oceanogr.,* **23,** 1553–1560.

Ferrari, R., and W. R. Young, 1997: On the development of thermohaline correlations as a result of nonlinear diffusive parameterizations. *J. Mar. Res.,* **55,** 1069–1101.

Gordon, A. L., 1991: The Southern Ocean: Its involvement in global change. *Proc. Int. Conf. on the Role of the Polar Regions in Global Change,* Fairbanks, AK, University of Alaska, Fairbanks, 249–255.

Jacobs, G. A., and J. L. Mitchell, 1996: Ocean circulation variations associated with the Antarctic Circumpolar Wave. *Geophys. Res. Lett.,* **23,** 2947–2950.

Jacobs, S. S., P. M. Bruchhausen, and E. B. Bauer, 1970: Eltanin reports cruises 32–36, 1968. Tech. Rep., Lamont Doherty Geological Observatory of Columbia University, Palisades, NY, 460 pp.

Johnson, G. C., and A. H. Orsi, 1997: Southwest Pacific Ocean water-mass changes between 1968/69 and 1990/91. *J. Climate,* **10,** 306–316.

Josey, S. A., E. C. Kent, and P. K. Taylor, 1998: *The Southampton Oceanography Centre (SOC) Ocean–Atmosphere Heat, Momentum, and Freshwater Flux Atlas.* Rep. 6, Southampton Oceanography Centre, 30 pp.

Kalnay, E., and Coauthors, 1996: The NCEP/NCAR 40-Year Reanalysis Project. *Bull. Amer. Meteor. Soc.,* **77,** 347–471.

Latif, M., and T. P. Barnett, 1994: Causes of decadal climate variability over the North Pacific and North America. *Science,* **266,** 634–637.

Manabe, S., and R. J. Stouffer, 1996: Low-frequency variability of surface air temperature in a 1000-year integration of a coupled ocean–atmosphere–land surface model. *J. Climate,* **9,** 376–393.

McCartney, M. S., 1977: Subantarctic mode water. *A Voyage of Discovery: George Deacon 70th Anniversary Volume* (supplement to *Deep-Sea Research*), M. V. Angel, Ed., Pergamon Press, 103–119.

——, 1982: The subtropical recirculation of mode waters. *J. Mar. Res.,* **40** (Suppl.), 427–464.

Metzl, N., B. Tilbrook, and A. Poisson, 1999: The annual fCO_2 cycle

and the air–sea CO_2 flux in the sub-Antarctic Ocean. *Tellus*, **51B,** 849–861.

Poisson, A., N. Metzl, C. Brunet, B. Schauer, B. Bres, D. Ruiz-Pino, and F. Louanchi, 1993: Variability of sources and sinks of CO_2 in the Western Indian and Southern Oceans during 1991. *J. Geophys. Res.*, **98,** 22 759–22 778.

Qiu, B., 2000: Interannual variability of the Kuroshio Extension System and its impact on the wintertime SST field. *J. Phys. Oceanogr.*, **30,** 1486–1502.

Reason, C. J. C., 2000: Multidecadal climate variability in the subtropics/midlatitudes of the Southern Hemisphere oceans. *Tellus*, **52A,** 203–223.

Ribbe, J., 1999: On wind-driven mid-latitude convection in ocean general circulation models. *Tellus*, **51A,** 505–516.

Rintoul, S. R., 1991: South Atlantic interbasin exchange. *J. Geophys. Res.*, **96,** 2675–2692.

——, and J. L. Bullister, 1999: A late winter hydrographic section from Tasmania to Antarctica. *Deep-Sea Res. I*, **46,** 1417–1454.

——, and S. Sokolov, 2001: Baroclinic transport variability of the Antarctic Circumpolar Current south of Australia (WOCE repeat section SR3). *J. Geophys. Res.*, **106,** 2795–2814.

——, and T. W. Trull, 2001: Seasonal evolution of the mixed layer in the subantarctic zone south of Australia. *J. Geophys. Res.*, **107,** 31 447–31 460.

——, J.-R. Donguy, and D. H. Roemmich, 1997: Seasonal evolution of upper ocean thermal structure between Tasmania and Antarctica. *Deep-Sea Res. I*, **44,** 1185–1202.

Roden, G. I., 1977: Oceanic subarctic fronts of the central Pacific: Structure of and response to atmospheric forcing. *J. Phys. Oceanogr.*, **7,** 761–778.

Rosenberg, M., R. Eriksen, and S. Rintoul, 1995: Aurora Australis marine science cruise AU9309/AU9391: Oceanographic field measurements and analysis. Research Rep. 2, Antarctic Cooperative Research Center, Hobart, Tasmania, Australia, 103 pp.

——, S. Bray, N. Bindoff, S. Rintoul, N. Johnson, S. Bell, and P. Towler, 1997: Aurora Australis marine science cruise AU9501, AU9604, and AU9601: Oceanographic field measurements and analysis, inter-cruise comparisons and data quality notes. Research Rep. 12, Antarctic Cooperative Research Center, Hobart, Tasmania, Australia, 150 pp.

Rudnick, D. L., and R. Ferrari, 1999: Compensation of horizontal temperature and salinity gradients in the ocean mixed layer. *Science*, **283,** 526–529.

Sabine, C., R. M. Key, K. Johnson, F. J. Millero, A. Poisson, J. Sarmiento, D. W. R. Wallace, and C. D. Winn, 1999: Anthropogenic CO_2 inventory of the Indian Ocean. *Global Biogeochem. Cycles*, **13,** 179–198.

Sloyan, B. M., and S. R. Rintoul, 2001a: Circulation, renewal, and modification of Antarctic mode and intermediate water. *J. Phys. Oceanogr.*, **31,** 1005–1030.

——, and ——, 2001b: The Southern Ocean limb of the global deep overturning circulation. *J. Phys. Oceanogr.*, **31,** 143–173.

Speer, K. G., S. R. Rintoul, and B. M. Sloyan, 2000: The diabatic Deacon cell. *J. Phys. Oceanogr.*, **30,** 3212–3222.

Sutton, R. T., and M. R. Allen, 1997: Decadal predictability of North Atlantic temperature and climate. *Nature*, **388,** 563–567.

Talley, L. D., 1996: Antarctic Intermediate Water in the South Atlantic. *The South Atlantic: Present and Past Circulation*, G. Wefer et al., Eds., Springer, 219–238.

——, 1999: Simple coupled midlatitude climate models. *J. Phys. Oceanogr.*, **29,** 2016–2037.

Thompson, R. O. R. Y., and R. J. Edwards, 1981: Mixing and water-mass formation in the Australian Subantarctic. *J. Phys. Oceanogr.*, **11,** 1399–1406.

Warren, B. A., 1972: Insensitivity of subtropical mode water characteristics to meteorological fluctuations. *Deep-Sea Res.*, **19,** 1–19.

Watterson, I. G., 2000: Southern midlatitude zonal wind vacillation and its interaction with the ocean in GCM simulations. *J. Climate*, **13,** 562–578.

White, W. B., and R. Peterson, 1996: An Antarctic Circumpolar Wave in surface pressure, wind, temperature and sea ice extent. *Nature*, **380,** 699–702.

——, S.-C. Chen, and R. Peterson, 1998: The Antarctic Circumpolar Wave: A beta effect in ocean–atmosphere coupling over the Southern Ocean. *J. Phys. Oceanogr.*, **28,** 2345–2361.

Wong, A. P. S., N. L. Bindoff, and J. Church, 1999: Large-scale freshening of intermediate waters in the Pacific and Indian Oceans. *Nature*, **400,** 440–443.

Yasuda, T., and K. Hanawa, 1997: Decadal changes in the mode waters in the midlatitude North Pacific. *J. Phys. Oceanogr.*, **27,** 858–870.

Young, W. R., 1994: The subinertial mixed layer approximation. *J. Phys. Oceanogr.*, **24,** 1812–1826.